Sedimentary Geology 223 (2010) 193–205

Contents lists available at ScienceDirect

Sedimentary Geology

journal homepage: www.elsevier.com/locate/sedgeo

Provenance of Lower Cretaceous Wölong Volcaniclastics in the Tibetan Tethyan Himalaya: Implications for the final breakup of Eastern Gondwana

Xiumian Hu [a,*], L. Jansa [b,1], Lei Chen [a,2], W.L. Griffin [c,3], S.Y. O'Reilly [c,3], Jiangang Wang [a,2]

[a] State Key Laboratory of Mineral Deposit Research, School of Earth Sciences and Engineering, Nanjing University, Nanjing 210093, China
[b] Geological Survey of Canada–Atlantic, Dartmouth, N.S., Canada
[c] GEMOC ARC National Key Centre, Department of Earth and Planetary Sciences, Macquarie University, Sydney, N.S.W. 2109, Australia

ARTICLE INFO

Article history:
Received 11 May 2009
Received in revised form 14 October 2009
Accepted 11 November 2009

Keywords:
Lower Cretaceous
Wölong Volcaniclastics
Provenance
Southern Tibet
Tethyan Himalaya
Greater India
Detrital zircon
U–Pb and Hf isotopes

ABSTRACT

Lower Cretaceous volcanic lithic arenites, widely distributed in the Tethyan Himalaya, provide insights into the continental breakup of Eastern Gondwana. In southern Tibet they are represented by the Wölong Volcaniclastics. The volcanic rocks that contributed clastic material to the lower parts of this unit were predominantly alkali basalts, whereas rhyolitic/dacitic volcanism becomes the predominant source of the upper strata. Geochemical analyses of basaltic grains and of detrital Cr-spinels from the Wölong Volcaniclastics demonstrate the alkaline character of the volcanism and suggest "within-plate" tectonic setting for the volcanism. Zircon U–Pb ages confirm that this volcanism continued from ~140 Ma to ~119 Ma. Hf-isotope data on these Early Cretaceous zircons indicate that their parental magmas were mantle-derived, but in the later stage of magmatic activity mantle-derived magmas were mixed with partial melts derived from the continental crust.

The Lower Cretaceous volcaniclastics occur along a broad belt paralleling the northern margin of Greater India. The onset of volcaniclastic deposition in the Himalayas appears to become progressively younger toward the west, but it ended synchronously during the Late Albian (~102 Ma). The low volume of volcanic rocks and their intra-plate tectonic setting suggest that they are the result of decompressional melting along extensional deep-seated fractures cross-cutting the continental crust, and reflect changes in regional intra-plate tectonic stresses when Greater India began to separate from the Australia–Antarctica supercontinent.

1. Introduction

The role of India in the dispersal of Gondwanaland remains poorly constrained due to complex tectonics along the Australian and Antarctic continental margins and the adjoining basins (e.g. Powell et al., 1988; Symonds et al., 1998; Heine et al., 2004; Ali and Aitchison, 2005, 2008; Gaina et al., 2007). Only limited paleomagnetic and marine geophysical data have been collected from surrounding oceanic lithosphere and basins, such as the Argo and Gascoyne Abyssal Plains off northwest Australian (Mihut and Müller, 1998; Heine et al., 2004) and the Enderby Basin, Princess Elizabeth Trough and Davis Sea Basin off the east Antarctic continental margin (Ramana et al., 2001; Gaina et al., 2007).

The Tethyan Himalaya, located between the Indus–Yarlung Zangbo Suture Zone to the north and the Higher Himalaya to the south, was part of the northern margin of Greater India continental plate during Cretaceous time (Hodges, 2000, Fig. 1a). Recent studies have advanced our understanding of the India–Asia collision processes (e.g. Leech et al., 2005; Najman et al., 2008), but few have focused on the pre-collision history, particularly on the breakup of Eastern Gondwana (Jadoul et al., 1998; Ali and Aitchison, 2005).

One key piece of evidence used in the reconstruction of the geotectonic evolution of Greater India is a major lithological change in the strata deposited around the Jurassic–Cretaceous boundary, and the related appearance of Lower Cretaceous volcanic arenites. These are known from several localities in the Tethyan Himalaya and include the Wölong Volcaniclastics outcropping in southern Tibet (Jadoul et al., 1998; Hu et al., 2006, 2008; Chen et al., 2007), the Pingdon La Formation in Zanskar, India (Garzanti, 1991), and the Kagbeni and Dzong Formations in Thakkhola, Nepal (Bordet et al., 1967; Gradstein et al., 1991; Dürr and Gibling, 1994; Garzanti, 1999). However, the age, magma compositions, magma sources and tectonic setting of the volcanic event(s) represented by the volcaniclastic sandstones remain poorly constrained.

In this paper we present new data on the Wölong Volcaniclastics in southern Tibet, including detailed petrological analyses, the chemical compositions of both volcanic grains and detrital Cr-spinels, and U–Pb

* Corresponding author. Tel.: +86 25 8359 3002; fax: +86 25 8368 6016.
E-mail addresses: huxm@nju.edu.cn (X. Hu), lujansa@nrcan.gc.cn (L. Jansa), bill.griffin@mq.edu.au (W.L. Griffin).
[1] Tel.: +1 902 426 2734.
[2] Tel.: +86 25 8359 3002; fax: +86 25 8368 6016.
[3] Tel.: +61 2 9850 8954; fax: +61 2 9850 8943.

0037-0738/$ – see front matter © 2009 Elsevier B.V. All rights reserved.
doi:10.1016/j.sedgeo.2009.11.008

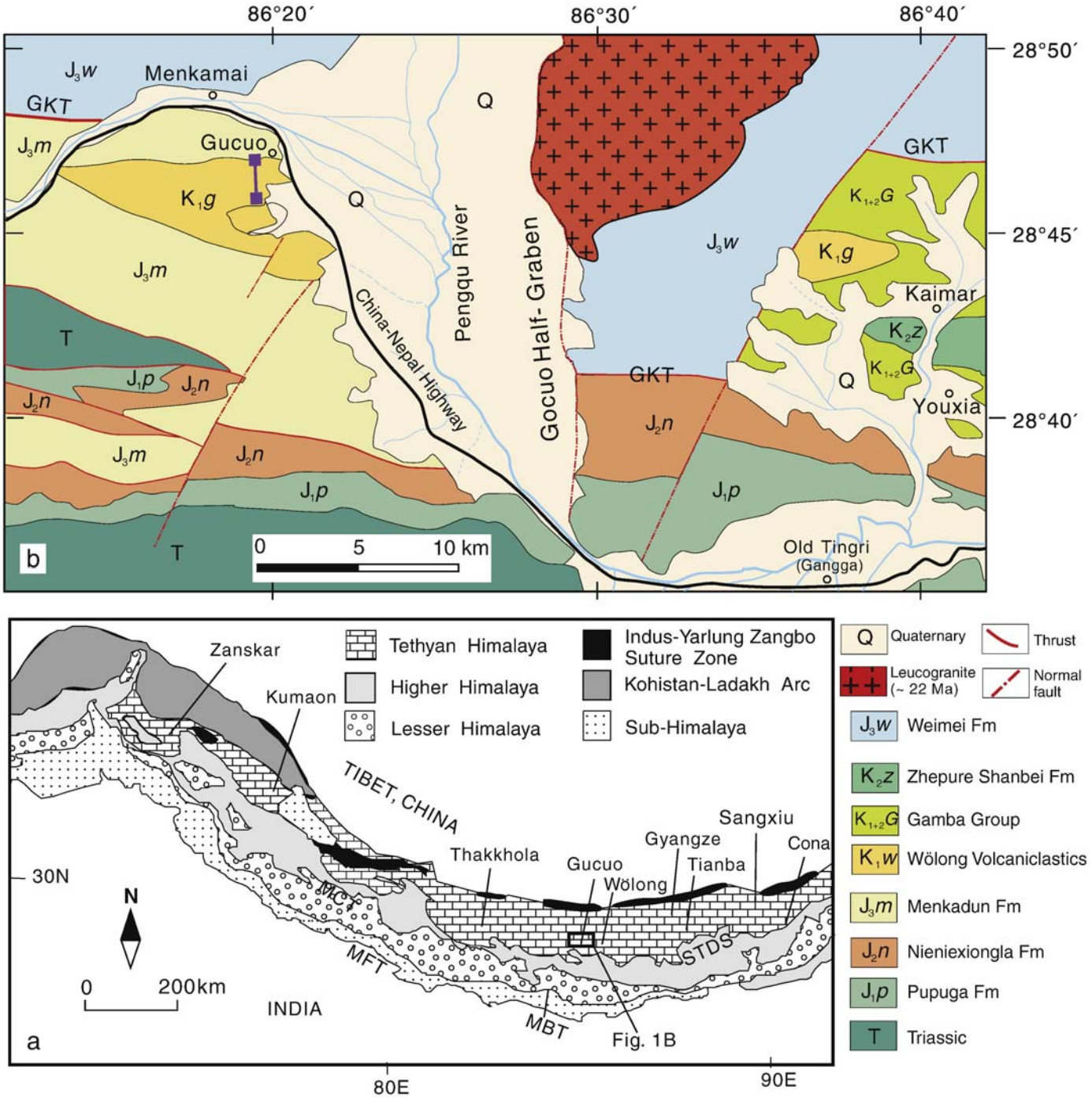

Fig. 1. a — Geological sketch map of the Himalayas, modified from Gansser (1964); MBT: Main Boundary Thrust; MCT: Main Central Boundary; MFT: Main Frontal Thrust; STDS: Southern Tibetan Detachment System; b — Geological map of the Gucuo area revised after Zhu et al. (2002). GKT — Gyirong–Kangmar Thrust.

ages and Hf-isotope analyses of detrital zircons. We discuss the implications of the new data for the sources of Early Cretaceous volcanism and the geologic processes affecting the northeastern margin of Greater India, and present a new geodynamic model to explain their occurrence.

2. Geological setting

Mesozoic strata exposed in the Tibetan Tethyan Himalaya (Gansser, 1964; Jadoul et al., 1998) (Fig. 1a) are subdivided into southern and northern zones along the Gyirong–Kangmar thrust (Ratschbacher et al., 1994). The southern zone is characterized by the presence of shallow-water (shelf) calcareous and terrigenous sedimentary rocks of Paleozoic to Eocene age (Liu and Einsele, 1994; Willems et al., 1996), whereas the northern zone is mainly dominated by Mesozoic to Paleogene deep-water sedimentary deposits of the outer shelf, continental slope and rise (Liu and Einsele, 1994; Hu et al., 2008). Here we present results of a detailed study of Lower Cretaceous volcaniclastic rocks from the Gucuo locality situated northwest of Old Tingri town (Fig. 1b). Tectonically, this area belongs to the northern zone of the Tibetan Tethyan Himalaya.

Mesozoic strata in the Gucuo area are exposed in several thrust sheets (Hu et al., 2008). They contain Upper Jurassic dark gray shales (Menkadun Formation) with abundant ammonites deposited in a shelf

environment (Jadoul et al., 1998; Yin and Enay, 2004). About 45 m-thick Gucuo Quartzarenite (Fig. 2), occurring in the upper part of the Menkadun Formation are white, thick-bedded, medium- to coarse-grained quarzitic sandstones that were deposited as near-shore sand bars and barriers (Hu et al., 2006). A fault separates the Menkadun Formation from the overlying Wölong Volcaniclastics (Fig. 2), which in study area are ~800 m thick. However, the strata are most probably strongly deformed by thrusting, which is difficult to resolve as the strata are only intermittently exposed. In the lower part of the Wölong Volcaniclastics sequence, the strata are composed of beds, up to 1 m thick, of fine to medium-grained volcaniclastic sandstones intercalated with gray shales and occasional pebbly conglomerates. The middle part is dominated by dark shales with thinner beds of siltstone and volcaniclastic litharenite. The volcaniclastic rocks are increasingly common toward the top. The upper part of the sequence begins with dark gray siltstones intercalated with fine-grained, upward-coarsening volcaniclastic sandstone beds, which become more frequent toward the top of the sequence. The presence of hummocky cross-stratification and mollusk coquinas in the upper part of the sequence indicate deposition on the shelf, with the sea floor occasionally exposed to storm-generated bottom currents (Hu et al., 2006). Ammonites, foraminifers and detrital zircon U–Pb ages (see below) suggest Aptian–Early Albian age for the Wölong Volcaniclastics (Hu et al., 2008). Paleoflow data for the Wölong Volcaniclastics through trough cross-beds measurements ($n=5$) yield a unidirectional, northerly paleoflow (NE15 to NW20) (Fig. 2).

The Upper Albian Dongshan Formation of the Gamba Group conformably overlies the Wölong Volcaniclastics (Fig. 2). It is composed of laminated gray calcareous shales, intercalated with siltstone beds that contain abundant siderite concretions. These strata were deposited in an offshore, deeper hemipelagic environment (Willems et al., 1996).

3. Samples and methods

Over 50 sandstone samples were collected at the Gucuo locality, situated at N28°46′56″, E86°19′13″, close to the China–Nepal

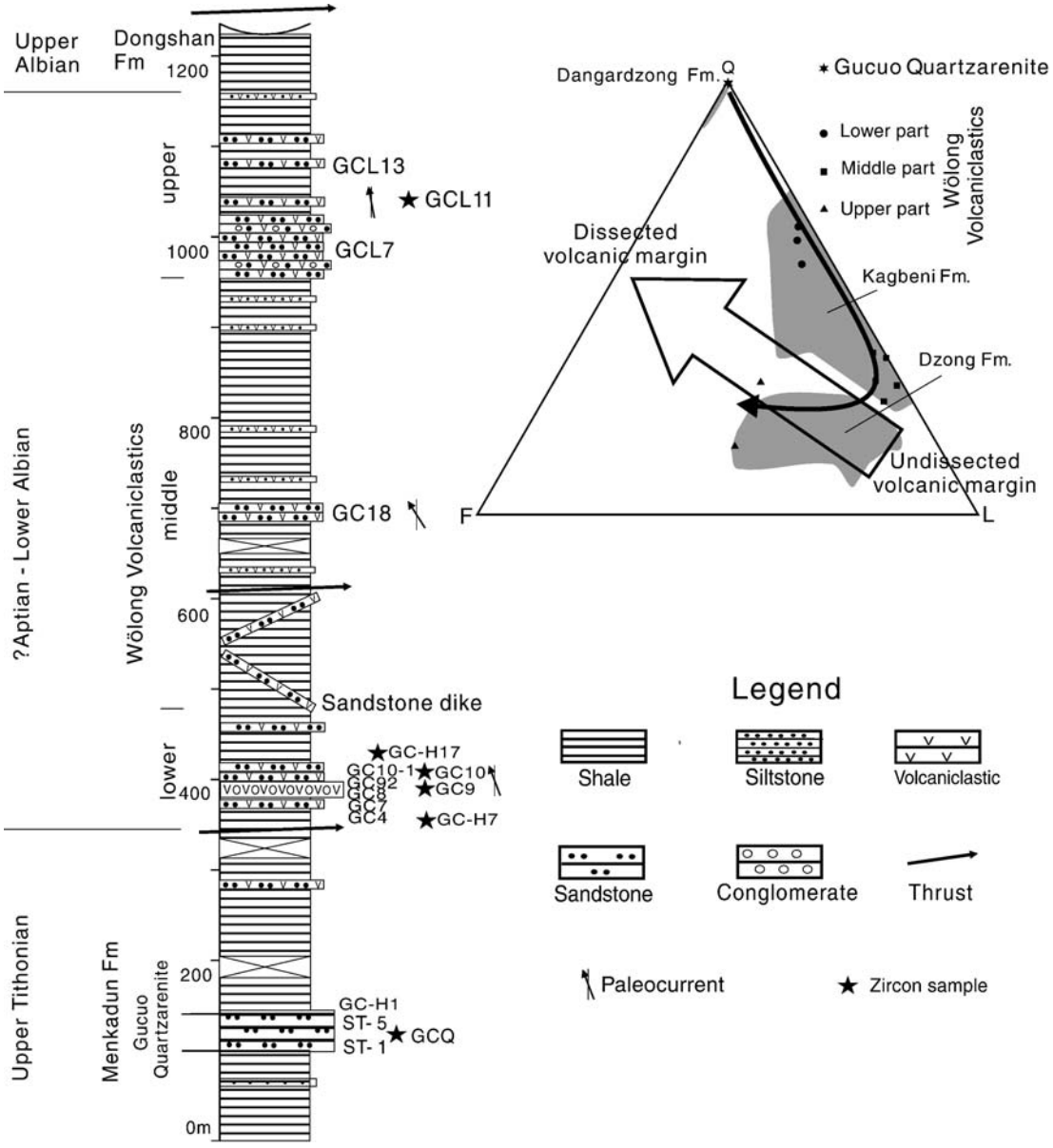

Fig. 2. Left: Generalized log of the stratigraphic section in the Gucuo area adapted from Hu et al. (2008), showing sample positions. Right: Detrital modes of the Gucuo sandstones, southern Tibet (modified from Chen et al. (2007)). Shaded area represents the compositions of the Dangardzong Fm, the Kagbeni Fm and the Dzong Fm at Thakkhola, Nepal (data from Dürr and Gibling (1994) and Garzanti (1999)). Evolution of detrital modes with progressive dissection of a volcanic refted margin was taken from Garzanti et al. (2001). Q = quartz; F = feldspars; L = aphanitic lithic fragments.

highway, 40 km northwest of Old Tingri (Gangga) in southern Tibet (Fig. 1b).

Polished thin sections were prepared from fine-grained conglomerates and coarse-grained Wölong Volcaniclastics. Volcaniclastic grains were analyzed for major elements by defocused (40 μm) beam microprobe (EMPA), using the approach of Dabard et al. (1994) (Appendix A1). For this study, we developed a new method using LA-ICPMS for the quantitative determination of major and trace elements in volcaniclastic grains in fine-grained conglomerates and coarse sandstones (see Appendix A2). One major advantage of this method is the capability for *in situ* sampling directly from thin section. This removes the need to isolate lithic clasts, an almost impossible task when dealing with sand-size, silica-cemented clastic rocks.

Seven sandstone samples (GCQ, GC-H1, GC-H7, GC09, GC10, GC-H17, and GCL11) were selected for the analysis of detrital heavy minerals (Fig. 2) (Appendixes A3, A4 and A5). Samples GCQ and GC-H1 are quartz arenites from the Gucuo Quartzarenite. Samples GC10 and GC-H17 were taken about 10 m above sample GC09; both are lithic arenites from the lower part of the Wölong Volcaniclastics (Fig. 2). GCL11 was taken from the upper part of the Wölong Volcaniclastics. Backscattered electron/cathodoluminescence (BSE/CL) images were made of zircon grains separated from the volcaniclastic rocks. *In situ* U–Pb dating of zircons and *in situ* Hf-isotope analyses were carried out, following the methods described by Jackson et al. (2004) and by Griffin et al. (2000), respectively.

Detailed descriptions of laboratory techniques used for major- and trace-element analyses of both volcanic grains and Cr-spinels by EMPA and LA-ICPMS, and the U–Pb dating and Lu–Hf isotope analysis of detrital zircon, are presented in Appendixes A1 to A5. All the analytical results are given in the Data Repository Table DR1-5.

4. Results

4.1. Sandstone composition and provenance

The Gucuo Quartzarenite located at the base of the studied sedimentary sequence (Fig. 2) is composed of 99% monocrystalline quartz grains, with trace amounts of K-feldspar, rutile and zircon. Quartz grains are moderately- to well-sorted and well-rounded, and cemented by silica (Fig. 3a), better preserved in the cold-cathodoluminescence photograph (Fig. 3b). On the tectonic discrimination diagram of Dickinson (1985) (Fig. 2; Chen et al., 2007), the Gucuo Quartzarenite plot in the field of "craton interior" sediments. In contrast, the stratigraphically higher sandstones of the Wölong Volcaniclastics (Fig. 2) are poorly- to moderately-sorted lithic arenites composed of subangular to subrounded monocrystalline quartz grains

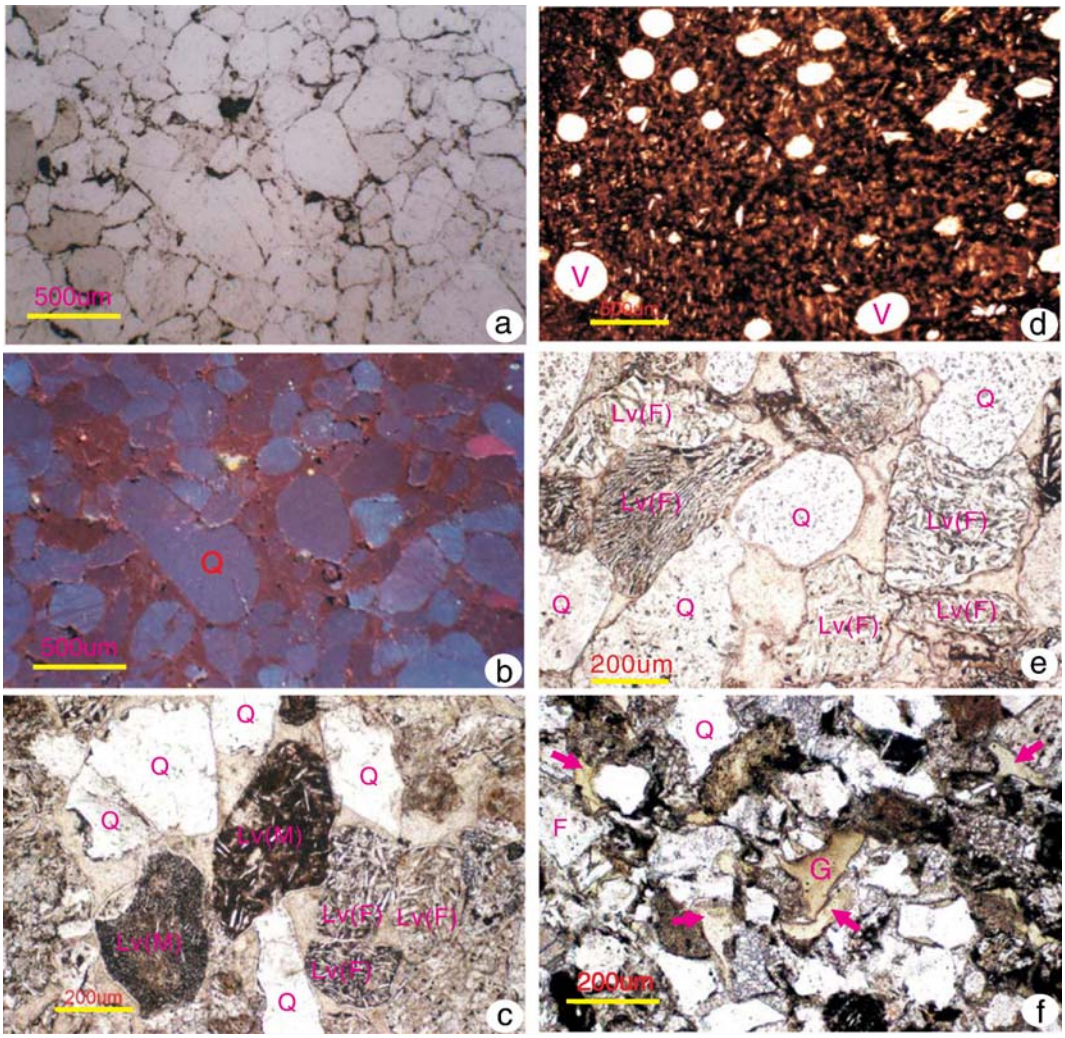

Fig. 3. Photomicrographs of sandstones from the Gucuo Quartzarenite and Wölong Volcaniclastics at Gucuo. a and b: polarized and cold-cathodoluminescence photographs of quartzose sandstone from the Gucuo Quartzarenite, showing the strong silica cementation (reddish color in b) between the quartz grains (bluish color in b); Sample GCH1, Gucuo; c and e: coarse sandstones of Wölong Volcaniclastics with abundant mafic volcanic lithics [Lv(M)] as well as felsic volcanic lithics [Lv(F)]. Sample GCB6, Gucuo; d: Numerous vesicles (V) within a basaltic grain as volcanic lithics from the Wölong Volcaniclastics, Sample GCB6, Gucuo; f: Volcaniclastic sandstone with abundant angular fragments of volcanic glass which are replaced by chlorite (G), indicating incorporation of volcanic ash. F: Feldspar.

(with minor polycrystalline quartz) and lithic volcanic fragments (31–68% of total grains) (Fig. 3c and b). Grains of sedimentary origin, such as siltstone and chert, occur in trace to minor amounts (0–14%).

In the lower part of the Wölong Volcaniclastics, the volcanic grains are predominantly of mafic composition (up to 55% of total volcanic grains) (Fig. 3c), showing pilotaxitic and trachytic texture, essentially devoid of K-bearing phases and of modal quartz. Measurement of extinction angles indicates that plagioclase within the basaltic volcanic grains is mainly oligoclase (An = 26–30), probably due to partial albitization during digenesis. Ovoid vesicles occur occasionally within basaltic grains (Fig. 3d). Felsic grains become relatively more abundant up-section, and are characterized by equigranular to slightly porphyritic microstructures (Fig. 3e).

In the upper part of the Wölong Volcaniclastics, feldspar grains comprise 28–40% of all grains. They are dominated by plagioclase, with significant amounts of microcline and K-feldspar showing perthitic and granophyric intergrowth; microcline and chessboard albite are rare. Measured extinction angles show that plagioclase compositions range from oligoclase to andesine (An = 24–31). Feldspar grains are angular, and K-feldspars are mostly fresh. The samples also contain grains with quenched-textured feldspars, indicating rapid cooling of the magma. The volcaniclastic sandstones in the upper part of the Wölong Volcaniclastics contain abundant volcanic glass fragments replaced by chlorite (up to 10%) (Fig. 3f). These could have been deposited *in situ* as volcanic ash fall from nearby volcanoes. Some of the volcanic grains are plastically deformed and squeezed between clastic grains, indicating that they were incorporated into the sediment in a plastic state, most probably as volcanic tuff particles. Vesicular texture was noted in a few basalt grains.

In the tectonic discrimination diagram for rifted-margin provenances of Garzanti et al. (2001), samples from the Wölong Volcaniclastics plot close to undissected volcanic margin (Fig. 2, Garzanti et al., 2001).

4.2. Chemical composition of volcanic grains

The EMPA analyses of volcanic grains from the Wölong Volcaniclastics show relatively low totals (84% to 97%) indicating that the grains are altered. This is supported by high Na_2O contents, and low K_2O, high Al_2O_3 and very low CaO, indicating chloritization and albitization of the volcanics. TiO_2 in volcanic grains is relatively high (mostly 2–4%, up to 5.1%). Albitization of plagioclase is indicated not only by EMPA analysis of feldspar laths within the volcanic grains, but also by the extinction angle analysis of plagioclase, demonstrating a predominantly oligoclase composition with An = 26–30.

When the geochemical data are plotted in the Total Alkali Silica (TAS) diagram of Le Maitre et al. (1989), the analyzed clastic grains from the Wölong Volcaniclastics fall into the fields of trachybasalt, basaltic trachyandesite, and trachydesite (Fig. 4). They are alkalic, rather than tholeiitic in composition. This classification may be distorted by the introduction of Na during albitization, but the Na introduction may be balanced by the apparent loss of K. In the Zr/TiO_2–Nb/Y diagram of Floyd and Winchester (1978), all volcanic grains except one classify as alkaline basalts (Fig. 5a). When compared with the TAS diagram (Fig. 4), the total contents of alkali elements may not have changed greatly. This indicates that the alteration affected the major elements more strongly than the trace elements. Despite the alteration, the concentrations of some less mobile trace elements enable a further discrimination of the volcanics. A within-plate tectonic setting is supported by high values of Nb and Zr, and to a lesser degree by the ratio of Ti to Y, as shown in Fig. 5c and d. The REE patterns of the samples show relative enrichments in LREE and depletion in HREE, suggesting a within-plate tectonic setting, similar to Oceanic Island Basalts (OIB) (Fig. 5b).

4.3. Chemical composition of detrital Cr-spinels

Cr-spinel is a ubiquitous accessory phase in basalts and peridotites. It has often been used as a sedimentary provenance

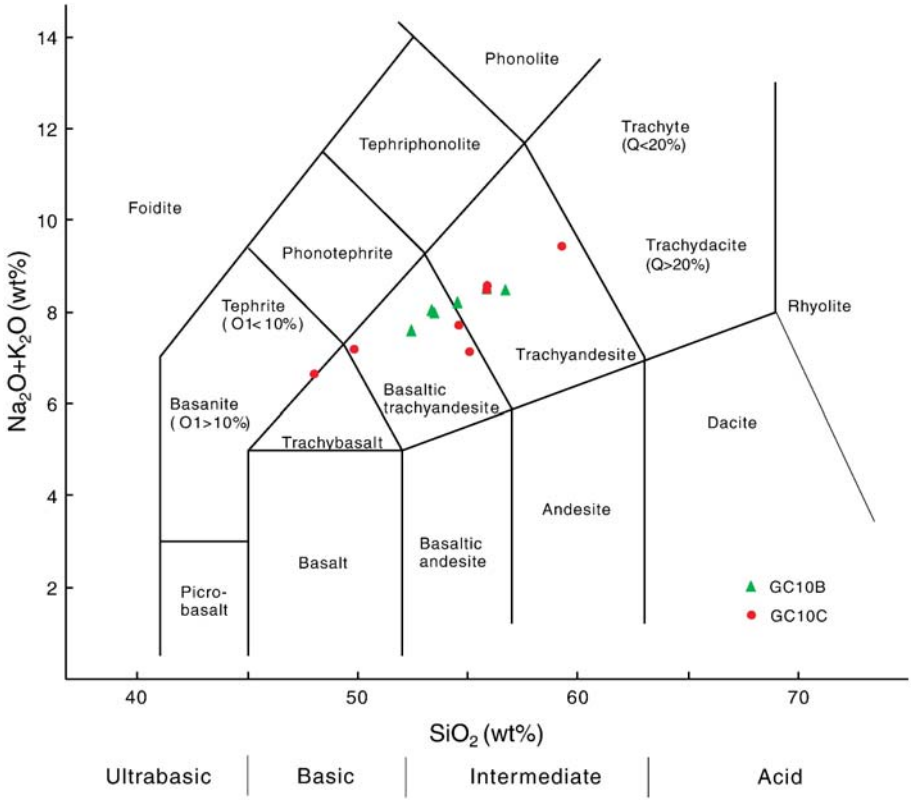

Fig. 4. Total Alkali–Silica (TAS) diagram (Le Maitre et al., 1989) showing the mafic volcanic grains from the Wölong Volcaniclastics. Major elements are obtained by both large-beam EMPA and LA-ICPMS methods (see Appendixes A1 and A2).

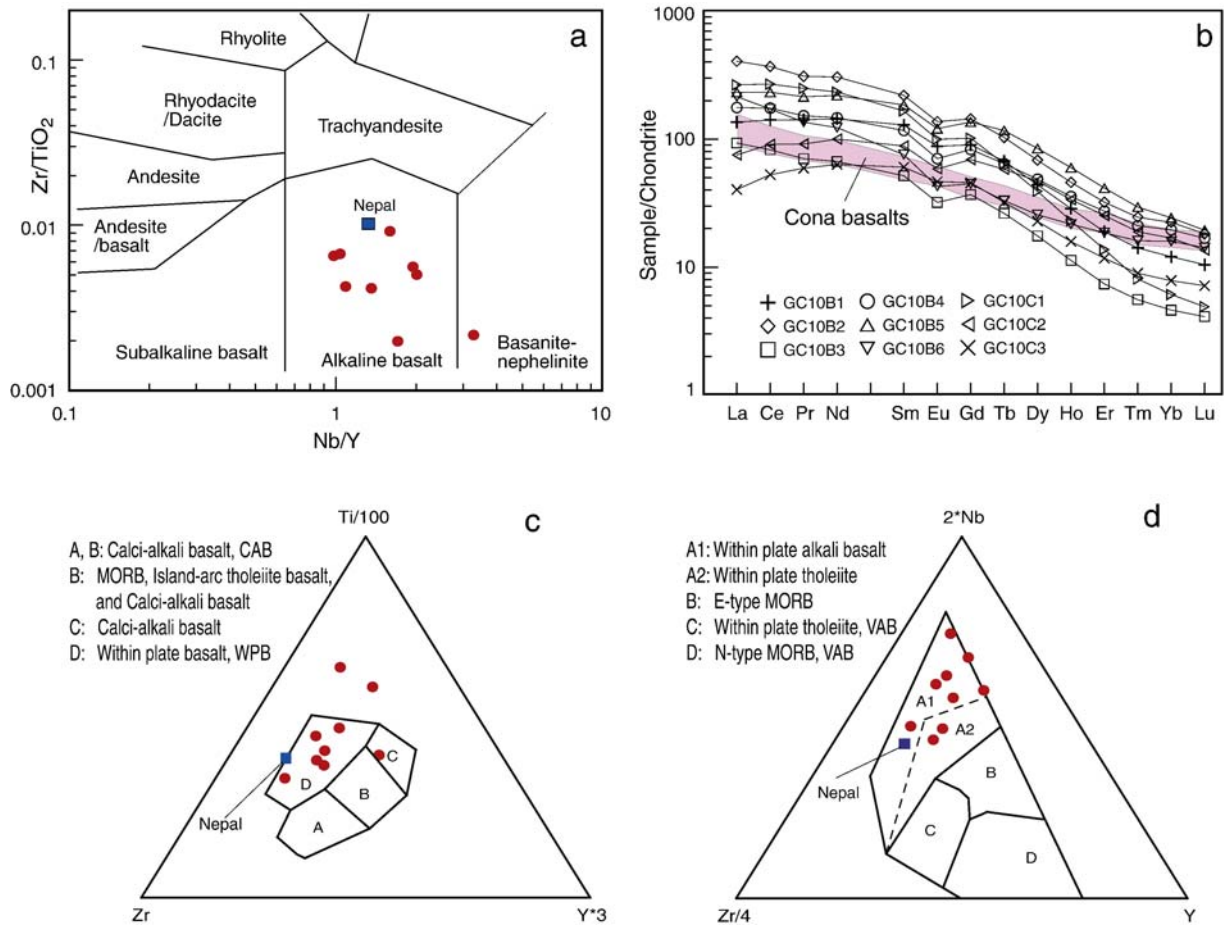

Fig. 5. Basalt discrimination diagrams showing the within-plate alkali-basaltic character of mafic volcanic grains from the Wölong Volcaniclastics. Data were obtained by LA-ICPMS. a) Nb/Y–Zr/TiO_2 diagram after Floyd and Winchester (1978). b) Chondrite — normalized REE patterns; data for chondrites are from Sun and McDonough (1989); REE data of Cona basalts are from Zhu et al. (2008); c) Ti/100 — Zr — Y 3 diagram after Pearce and Cann (1973); d) 2 Nb — Zr/4 — Y diagram after Meschede (1986).

indicator due to its compositional variation and its physical and chemical durability (Lenaz et al., 2000). Most spinels from residual mantle peridotites tend to have low TiO_2 contents (<0.2%) and have higher Fe^{2+}/Fe^{3+} (>10) than spinels from volcanic rocks (Kamenetsky et al., 2001). The TiO_2 contents and $Fe^{2+}/Fe3^{+}$ ratios of detrital Cr-spinels from the Gucuo section (samples GC-H1 and GC-

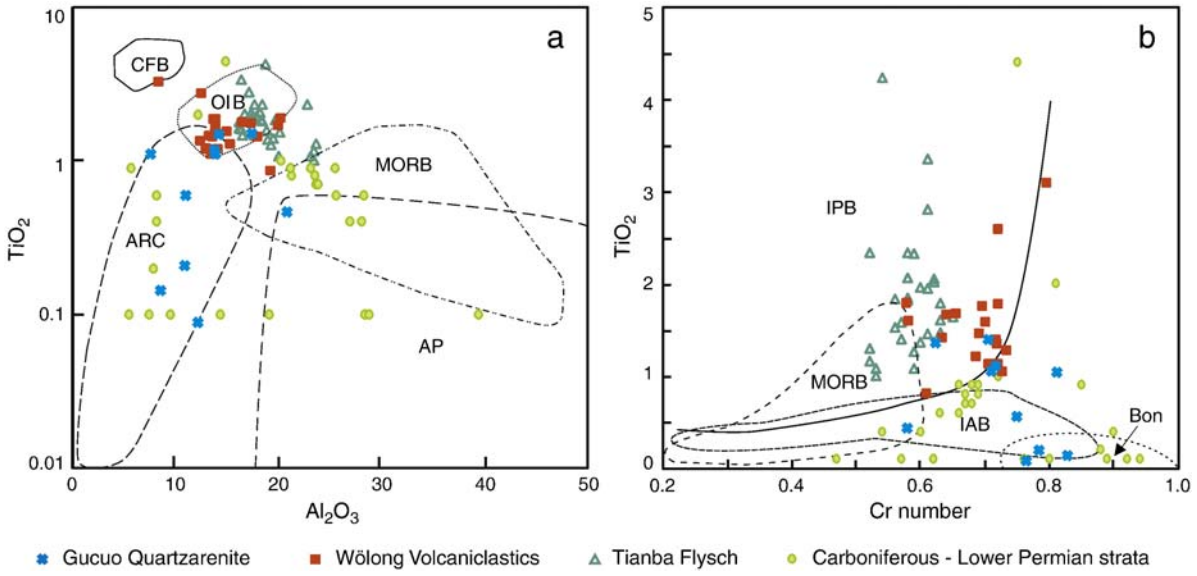

Fig. 6. Tectonic setting discriminant plots for spinels from the Gucuo section. (a), TiO_2 versus Al_2O_3 after Kamenetsky et al. (2001); (b) TiO_2 versus Cr number [Cr/(Cr + Al)] after Arai (1992). Data for spinels in the Tianba Flysch and Carboniferous–Lower Permian strata in Tethyan Himalaya are from Zhu et al. (2004), Sciunnach and Garzanti (1997), respectively. AP, Abyssal peridotite; BABB, Back-arc basin basalt; Bon, Boninite; CFB, Continental flood basalt; IAB, Island arc basalt; IPB, Intra-plate basalt; MORB, Mid-oceanic ridge basalt; OIB, Ocean island basalt.

H17) are mostly >0.2% and <10%, respectively, suggesting a volcanic origin — mostly probably basaltic (Lenaz et al., 2000; Kamenetsky et al., 2001) (Table DR3).

Cr-spinels from variety of types of mafic and ultramafic rocks can be discriminated by various chemical parameters (e.g. Dick and Bullen, 1984; Arai, 1992). Tectonic setting discrimination plots – binary plots of TiO_2 versus Al_2O_3, and TiO_2 versus Cr number [Cr/(Cr + Al)] – show that the compositional range of the detrital spinels from the Wölong Volcaniclastics most closely matches that of spinels from oceanic island basalts (OIB) or intra-plate basalts (Fig. 6), and excludes island arc basalts, mid-ocean ridge basalt (MORB), boninites and ophiolites as significant sediment sources. The compositional ranges of the detrital spinels from the underlying Gucuo Quartzarenite have low TiO_2 value, very similar to those from Carboniferous–Lower Permian strata in Tethyan Himalaya (Fig. 6, Sciunnach and Garzanti, 1997). As this area represents a relatively stable marine environment, and no igneous activities are known from Early Permian to Late Jurassic, we suggest that detrital spinels from the Gucuo Quartzarenite most probably are derived from the same or similar ones to source rocks as those in the Carboniferous–Lower Permian strata in the Tethyan Himalaya.

4.4. U–Pb ages of detrital zircon

Seventy-two zircon grains from sample GC-H7 from the lowermost of the Wölong Volcaniclastics, 46 zircon grains from sample GC09 and 70 grains from sample GC10 (both in the lower part) and 70 grains from sample GCL11 (from the upper part) were dated by the U–Pb method (Table DR4). Among the 234 acceptable analyses (Table DR4), 64% have Th/U ratios >0.4 (up to 8.8), and 8% have Th/U<0.2 (as low as 0.02), indicating that most grains are magmatic in origin (Wu and Zheng, 2004). The Th/U ratios of all 32 zircon grains with an Early Cretaceous age are >0.4 (0.5 to 4.4), indicating a probable magmatic origin. All of these grains exhibit homogenous internal structure in BSE/CL images, with no overgrowths.

The most striking feature of the U–Pb analyses of zircons from the Wölong Volcaniclastics is the presence of Early Cretaceous age peaks (Figs. 7 and 8), ranging from 119 ± 2 Ma to 140 Ma ± 4 Ma (1σ), with a median age of about 126.5 Ma (Fig. 8). The youngest U–Pb age constrains the maximum depositional age to ~119 ± 2 Ma (1σ) for the Wölong Volcaniclastics, which corresponds to the Aptian on the time scale of Gradstein et al. (2004). It is interesting to note that the relative abundance of the Early Cretaceous U–Pb ages increases significantly from 3% in the lowermost part of the section (GC-H7), 13–14% in the lower part (samples GC09 and GC10) to 28% (sample GCL11) in the upper part of the Wölong Volcaniclastics. This increase in the abundance of Early Cretaceous zircons correlates with an increased proportion of volcanic detritus in the sandstones higher in the section.

The second zircon population in the Wölong Volcaniclastics is Early Paleozoic in age (479 Ma to 544 Ma; Fig. 7). This Cambro–Ordovician zircon population has previously been documented in the Lower Paleozoic Tethyan Himalaya sequences by Gehrels et al. (2003, 2006) and Myrow et al. (2009), and attributed to Early Palaeozoic orogenesis along the Indian margin of Gondwana (Garzanti et al., 1986; Gehrels et al., 2003; Cawood et al., 2007). Precambrian zircons (77% of grains) from the Wölong Volcaniclastics are dominated by a broad cluster between 730–1000 Ma (peaks at 824 Ma and 978 Ma), with small clusters at 1060–1210 Ma and 2430–2730 Ma (Fig. 7). Nine Archean zircons with ages ~3.0–3.3 Ga were also found (Fig. 7).

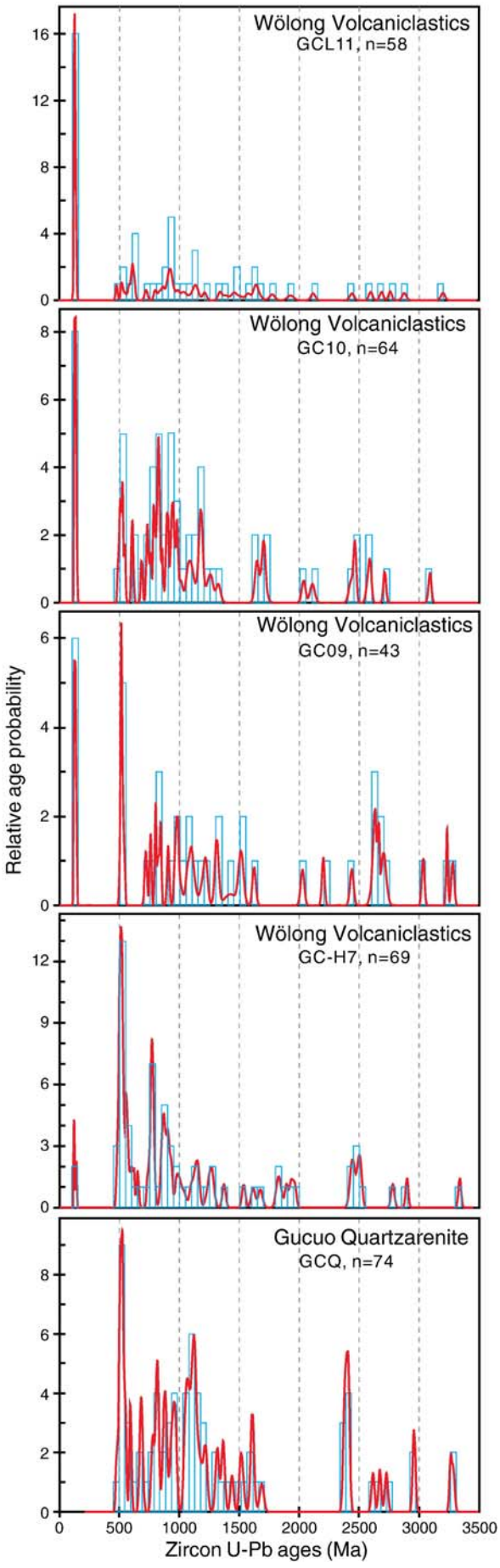

Fig. 7. Relative probability plots of U–Pb data. Sample GCQ was taken from the Gucuo Quartzarenite at Gucuo; samples GC09 and GC10 were taken from the lower part of the Wölong Volcaniclastics at Gucuo; sample GCL11 was taken from the upper part of the Wölong Volcaniclastics at Gucuo.

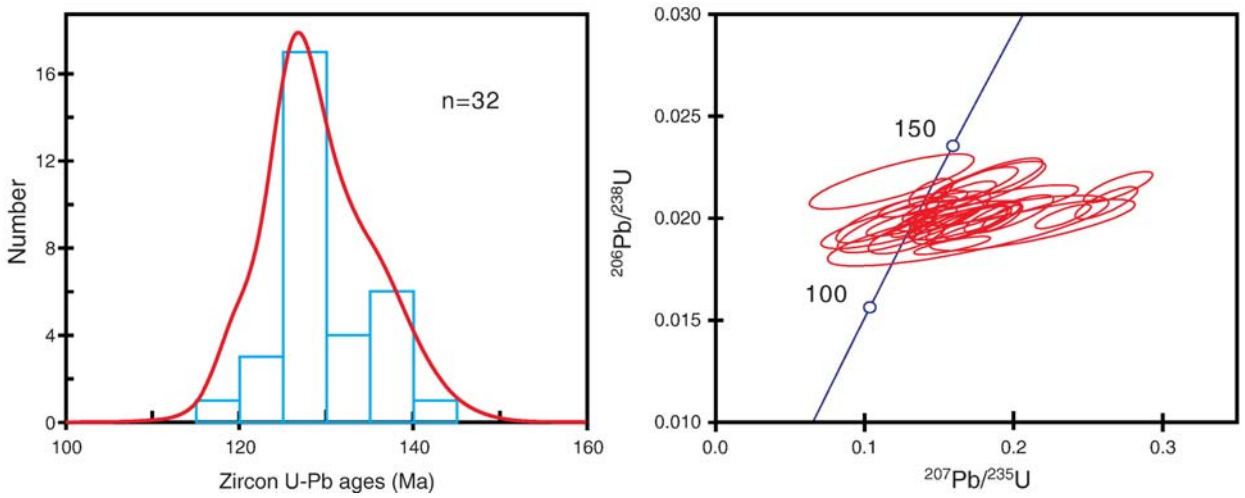

Fig. 8. Histogram and cumulative probability curve (left) and Pb/U Concordia diagram (right) of detrital zircon grains of Early Cretaceous age from Wölong Volcaniclastics.

Sample GCQ of 83 zircon grains from the underlying Gucuo Quartzarenite shows similar pattern of zircon ages to those from the Wölong Volcaniclastics, except that the Early Cretaceous zircon population is absent (Fig. 7). The most prominent zircon age population from sample GCQ is Cambro–Ordovician (482–558 Ma).

4.5. Hf isotopes in detrital zircon

Eighty dated zircon grains from the Wölong Volcaniclastics were further analyzed for Hf isotope ratios (Table DR5), with three populations of detrital zircons defined (Fig. 9). The $\varepsilon_{Hf}(t)$ of the Early Cretaceous zircons ($n=12$, 15% of total analyzed grains) ranges from −1.5 to −7.2 with an average of −4.6. T^C_{DM} model ages, which help to constrain the age of the source rocks for the melts, range from 1.3 to 1.6 Ga.

Most zircons with U–Pb ages of 0.5–1.7 Ga ($n=55$, 69%) have T^C_{DM} model ages of 1.5–2.9 Ga. Two grains (601 Ma and 610 Ma) have positive $\varepsilon_{Hf}(t)$ of +1.4 and +6.4, and T^C_{DM} model ages of 1.2 Ga and 1.5 Ga (Fig. 9). As shown in Fig. 9, the origin of these 0.5–1.7 Ga zircons is consistent with repeated remelting of 1.7–2.4 Ga continental crust. Only the ~610 Ma zircons would require significant addition of juvenile material.

The zircons with U–Pb ages of 2.0–3.3 Ga ($n=13$, 16%) have T^C_{DM} model ages of 2.1–3.7 Ga (Fig. 9). This population of detrital zircons is consistent with production of the host magmas by melting 2.8–3.5 Ga juvenile continental crust (Fig. 9).

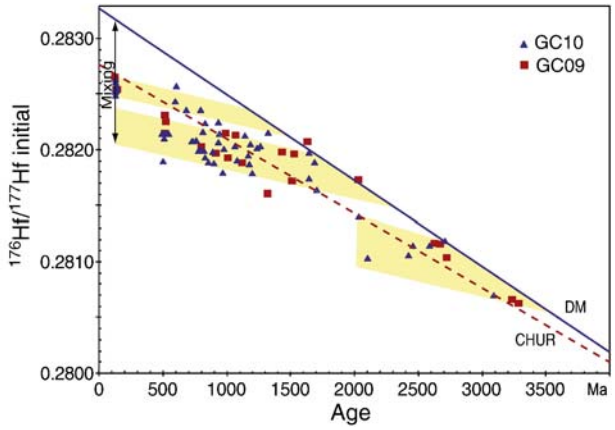

Fig. 9. Plot of $^{176}Hf/^{177}Hf$ versus U–Pb age of analyzed zircons from the Wölong Volcaniclastics.

5. Discussion

5.1. Provenance and tectonic setting of the Wölong Volcaniclastics

The petrological composition of mostly monocrystalline quartz suggests that the Gucuo Quartzarenite was most probably recycled from the Indian "craton". The age distribution of detrital zircons from the Gucuo Quartzarenite supports this interpretation showing age populations very similar to those obtained from older Cambrian–Devonian sequences in the Tethyan Himalaya (Gehrels et al., 2003) (Fig. 7).

The source area of the volcanic material in the Wölong Volcaniclastics had to be located to the south of the Gucuo area, since the trough cross-beds measurements in the sandstones document a unidirectional, northerly paleoflow (Fig. 2), similar to those in both the Kagbeni area of northern Nepal (Bordet et al., 1967; Gradstein et al., 1991; Dürr and Gibling, 1994) and the Zanskar area of India (Garzanti, 1993). The volcanic and terrigenous clastic grains are generally poorly sorted, and moderately reworked. These features suggest that some, if not all, of the volcanics were subaerially erupted, but the volcanic center was not far from the coast. The presence of volcanic tuff particles (Fig. 3f), the unweathered nature of some of the volcanic grains and feldspars and the angular to subangular shape of most of the volcanic and quartz grains all indicate rapid erosion and relatively short transport.

The Wölong Volcaniclastics have a detrital zircon age distribution very similar to that of the underlying Gucuo Quartzarenite, but with the addition of an Early Cretaceous zircon population (Fig. 7). Combined with compositional data together, we interpreted that the Wölong Volcaniclastics have a mixed sediment source, with material derived both from the Indian cratonic interior and from a new source of Lower Cretaceous volcanic rocks, which was situated south of the Gucuo locality along the northern Greater Indian margin.

Our geochemical data of volcanic grains from the Wölong Volcaniclastics (Section 4.2) let us draw two conclusions: Firstly, they are alkalic (Fig. 5a), rather than tholeiitic in composition; secondly, they are situated in a within-plate tectonic setting, as evidenced by high values of Nb and Zr, to a lesser degree by the ratio of Ti to Y, and relative enrichments in LREE and depletion in HREE (Fig. 5b). The chemical composition of detrital Cr-spinels from the Wölong Volcaniclastics also supports an intra-plate tectonic setting (Fig. 6). Moreover, the Hf-isotope data indicate that the parent magmas of the Early Cretaceous zircons contain a significant crustal component and reflect mixing between magma ascending from the mantle and partial melts of the old continental crust (Fig. 9), compatible with an intra-plate extensional setting.

5.2. Potential source of volcaniclastic material

The presence of Lower Cretaceous volcaniclastic sediments in the Tethyan Himalaya was previously thought to reflect obduction of ophiolites to the north of the area during the Himalayan collision (Gansser, 1964). However, the prevailing northward paleocurrent directions and the within-plate alkali-basaltic character of the mafic volcanics do not support an ophiolite source. Later studies, e.g. Gradstein et al. (1991) have suggested that the source was the alkalic Aulis volcanics in the Tansen area of the Lesser Himalaya. However, these rocks consist of phonotephrites and trachytes, rather than basalts (Sakai, 1983). They also yield Rb/Sr biotite–feldspar ages of 96.7 ± 2.8 Ma (Sakai et al., 1992), which would make them too young to be a source for the Wölong Volcaniclastics.

In eastern India, the Rajmahal Traps consist mainly of quartz-normative tholeiites with maximum exposed thickness of lava over 230 m (Kent et al., 1997). Pb–Nd–Sr isotopic ratios and trace element data (Kent et al., 1997) for the Rajmahal basalts indicated a hotspot origin from a material input similar to Kerguelen basalts. $^{40}Ar/^{39}Ar$ dating on whole-rocks (Kent et al., 2002) indicated that the Rajmahal Traps were emplaced at ~118 Ma, while dykes intruded to the Rajmahal Traps appear to be 2–3 Myr younger than basaltic lava. The OIB-type and its young age of the Rajmahal Traps ruled out its potential source for the Wölong Volcaniclastics.

Recently, volcanic rocks have been found in the Sangxiu–Cona area of southeastern Tibet, within the Northern Zone of the Tethyan Himalaya (Fig. 1a), where they are interbedded with Upper Jurassic–Lower Cretaceous deep-water sedimentary strata (Fig. 1a) (Zhu et al., 2005b, 2007, 2008). The Sangxiu–Cona volcanic rocks mainly consist of mafic alkali basalts, diabase, gabbroic diabase and felsic volcanic rocks such as dacite. They have been dated by SHRIMP U–Pb analysis of zircon to 144.7 ± 2.4 Ma and 131.1 ± 6.1 Ma (diabase from Cona) and 133 ± 3.0 Ma (dacite from Sangxiu; Zhu et al., 2005a,b, 2008). The thickness of the basalts ranges from several meters to 614 m. Major-element, trace-element and Sr–Nd isotopic compositions of the basalts were interpreted by Zhu et al. (2007) to indicate an OIB-type mantle source, with discernable contributions from the subcontinental lithospheric mantle (SCLM). Since the Sangxiu–Cona volcanics are located within the deep marine environment of the Northern Zones and more than 300 km east of Gucuo (Fig. 1a), they are unlikely to be a source for the Wölong Volcaniclastics. Their occurrence suggests that other Lower Cretaceous volcanic centers may have been present in the Northern Zone and similar volcanic centers may have existed further to the south, but, intra-plate volcanic rocks with 140–120 Ma age are unknown from the Lesser Himalayan tectonic zone. If such volcanic centers existed, they were probably either eroded away, or were destroyed by tectonic processes during the Himalayan orogenesis, or were buried by younger Himalayan foreland sediments.

5.3. Geotectonic model for the early Cretaceous volcanic event

In southern Tibet, the Wölong Volcaniclastics was firstly described by Jadoul et al. (1998) near Wölong village along the road from Tingri to Everest base camp (Fig. 1a). These more than 400 m-thick succession deposited in delta-shelf environments are mainly composed of volcanic arenites and mudrocks, and have been biostratigraphically assigned to the lowermost Tithonian to uppermost Aptian (Jadoul et al., 1998). In the Gyangze area of the Northern Tethyan Himalaya (Fig. 1a), the 73 m thick Rilang Formation of Early Cretaceous deposited in deep-water environment is composed of gray shales intercalated with subarkosic and sublitharenitic sandstones that contain volcanic grains near the top of the formation (Hu et al., 2008). The early- to mid-Cretaceous Tianba Flysch near Kangmar (Zhu et al., 2004) (Fig. 1a) is about 220 m thick and consists primarily of deep-water sandstone, siltstones, and shales. Sandstones in the lower part are primarily quartz-rich lithic arenites, whereas sandstones in the upper part are lithic wackes with feldspar and volcanic lithic clasts and a few metamorphic lithics. Zhu et al. (2004, 2005a) concluded that the detrital Cr-spinels in the Tianba Flysch were derived from intra-plate basalts, rather than from arc-complexes or ophiolites.

The presence of Lower Cretaceous volcaniclastic rocks similar to the Wölong Volcaniclastics has been documented at several localities in western Himalaya (Fig. 1a), including Zanskar Himalaya (Garzanti, 1991), Malla Johar area of the Kumaon Himalaya in India (Kumar et al., 1977; Sinha, 1989), and Thakkhola area of Nepal Himalaya (Bordet et al., 1967; Gradstein et al., 1991; Gibling et al., 1994; Dürr and Gibling, 1994; Garzanti, 1999). Regional correlation of the above occurrences shows that the onset of deposition of volcaniclastic sandstones and thus the volcanic eruptions in the northern Greater Indian margin, is diachronous (Hu et al., 2008). It may have started as early as Tithonian in the eastern Himalaya (Gibling et al., 1994; Nagy et al., 1995; Jadoul et al., 1998) and progressed westward along the northern edge of Greater India, and terminated during Albian time in the Zanskar Himalaya (Garzanti, 1993). However, the Lower Cretaceous volcaniclastic sedimentation ended synchronously in the Late Albian (the planktonic foraminifera of the *Rotalipora subticinensis* Subzone, 101.7–102.4 Ma of Leckie et al. (2002)) all along the northern margin of Greater India from Zanskar to Nepal and further to southeastern Tibet (Premoli Silva et al., 1991; Garzanti, 1993; Gibling et al., 1994; Garzanti, 1999; Hu et al., 2008). A deep-water hemipelagic or pelagic environment was established soon after the Lower Cretaceous volcaniclastic deposition in latest Albian time (*R. appenninica* Zone) including the Chikkim/Fatu La in Zanskar (Garzanti, 1993; Bertle and Suttner, 2005), the Muding Formation in Nepal (Gibling et al., 1994; Garzanti, 1999) and the Dongshan Formation of the Gamba Group (Willems et al., 1996) in southern Tibet. This drowning of the Indian passive margin has been ascribed to thermal cooling of the crust, continental margin subsidence and waning of sediment supply to the margin edge after the magmatic event (Garzanti, 1993; Dürr and Gibling, 1994).

Any tectonic model attempting to explain the origin of the Early Cretaceous volcanism along the northern margin of Greater India should consider: 1) the intra-plate tectonic setting; 2) its nearly linear distribution along the northern margin of Greater India; 3) the diachronous onset of volcanicity with westward migration, but synchronous termination; and 4) mantle-derived magmas mixed with melts of older, probably mid-Proterozoic crust as suggested by detrital zircon Hf isotopes.

Two different geodynamic hypotheses have been previously proposed to explain the origin of the Early Cretaceous volcanic event along the northern margin of Greater India: 1) it is a rift-related volcanism, triggered when Greater India begins to separate from the East Gondwana (Antarctica and Australia) supercontinent (Gaetani et .al., 1986; Gradstein et al., 1991; Garzanti, 1993, Dürr and Gibling, 1994); and 2) it is the product of a propagating hot spot and mantle plume (Zhu et al., 2004, 2007).

We consider the plume hypotheses to be inadequate for the following reasons. Early Cretaceous volcanic centers occur in a long belt (over 1500 km) paralleling the paleo-margin of Greater India, with mafic volcanism restricted to a few volcanic centers. The volume of magma produced is low, and of alkaline composition, with the direction of the belt oriented almost perpendicularly to the track of the Kerguelen hot spot (Kent et al., 2002; Coffin et al., 2002); the major magmatic activity on Kergulen is dated as 120–110 Ma (see Coffin et al., 2002), and therefore it is younger than the igneous activity on the northern Greater Indian margin.

The alternative hypothesis that volcanicity is the result of rifting has been based only on a recognition that the volcanism is intra-plate and alkaline in composition. But was there a rift? Rifting processes as broadly understood involve thermal doming and uplift and stretching of the crust, accompanied by faulting, igneous activity and rapid

deposition in moderately deep, elongated, fault-bounded troughs (Manspeizer, 1988). The drift or post-drift stage involves slow cooling and subsidence of the plate over a wide area, and hence it is marked by stratigraphic onlap over a broad terrain of eroded rift basins lying on thinned continental and rift-stage crust (Manspeizer, 1988). Such processes are well documented from the Mesozoic rifting of the African and North American plates, involving cratonic breakup and rift basin evolution on both sides of the North Atlantic Ocean. However, the paleogeographic reconstruction of Gondwana in Jurassic time (e.g. Ali and Aitchison, 2008) shows that to the northeast of the Greater Indian margin, where the Early Cretaceous volcanic centers are located, was a deep ocean, most probably floored by oceanic crust. In a reconstruction of Greater India, Ali and Aitchison (2005) suggested that the central portion of the Indian continent probably extended not more than 950 km, while Gaina et al. (2003) suggest extension of only 400 km. Studies of the Lower Cretaceous sedimentary strata in southern Tibet (Willems et al., 1996; Jadoul et al., 1998) and northern Nepal (Gradstein et al., 1991; Gibling et al., 1994) provide strong evidence that the Aptian volcaniclastic sequence is overlain by deeper-shelf shaly beds, with the Late Albian hemipelagic sediments being already deposited on the upper continental slope. Therefore an open, deep oceanic basin lay northeast of the Greater Indian margin, as shown in the plate reconstruction of Ali and Aitchison (2008).

The deposition of the volcaniclastic sandstones on the shelf further indicates that there could not be any rift basin located in the hinterland, which otherwise would trap the volcaniclastic sandstones. However, the occurrence of volcaniclastic sandstones sandwiched between predominantly shaly shelf strata at Kagbeni as well as at Gucuo indicates that the volcanic activity was probably accompanied by minor uplift, which results in weathering and transporting of the volaniclastical materials.

The geochemical analyses demonstrate that the volcanicity is of intra-plate (intra-continental) affinity. We agree that it was triggered by continental extension-related to Australia–India plate separation, but it does not necessarily indicate a rifting event on the northern Greater Indian margin. The evolution of the western Australian margin documents extensive volcanic activity from about 155 Ma at Argo Abyssal Plain to about 131 Ma (Valanginian, Müller et al., 1998) in the Perth abyssal plain to the Naturaliste Plateau in the south (Symonds et al., 1998). South of the Plateau the margin is volcanic, represented by the continental Bunbury basalt, inferred to be similar in age to Perth Basin dolerites dated at 136 ± 3 Ma (Davies et al., 1989). We consider the Bunbury basalt to be possibly correlative and to represent the most south- eastern termination of the Early Cretaceous igneous volcanic belt of the Indian margin (Fig. 10).

We propose that the geotectonic setting of the Early Cretaceous volcanic activity on the northern India continental margin can be explained by a leaky deep-seated fault model (Fig. 10). In this model, rifting of Greater India from the Antarctica–Australia supercontinent resulted in changes in the direction of the regional stress-field, particularly along the northeastern margin of the Greater India continental plate, as previously suggested by Powell et al. (1988). The unzipping of the Greater India continental plate from the Australia/Antarctica plate was accompanied by minor counterclockwise rotation (Ali and Aitchison, 2008). This led to the formation and opening of deep-seated fractures, which cross-cut the continental crust and propagated northwest along the margin. This fracturing allowed decompression melting and the rise of mantle-derived basaltic magma, in later stages mixed with partial melts of continental crust (Fig. 10).

This model with northwest propagating, extension-related deep-seated fractures can account for all of the features of the Early Cretaceous evolution of the Tethyan Himalaya that we have listed above. We suggest that the opening of these fractures initially began in the eastern Himalaya in about Tithonian time, progressed slowly westward and reached the Zanskar Himalaya in the Late Albian. When Greater India finally separated from the Australia–Antarctica supercontinent and started to drift away, probably in Late Albian time (~102 Ma), the igneous activity ceased as the continental extension ceased and the Greater India continental plate became free.

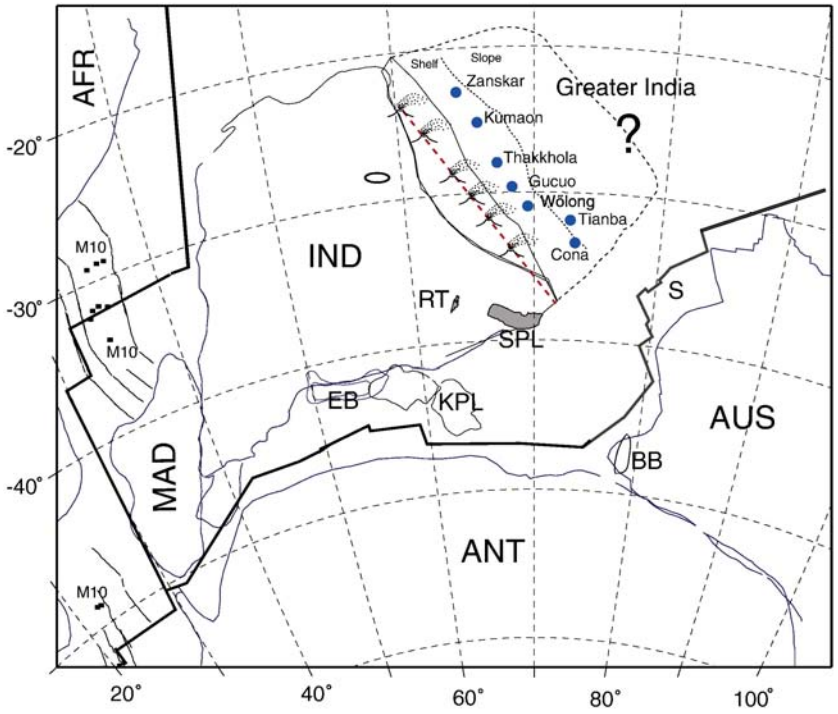

Fig. 10. Indian Ocean plate reconstructions at 126.7 Ma revised from Kent et al. (2002). Bold lines indicate assumed positions of plate boundaries. Fine lines represent continental coastline. AFR, Africa; ANT, East Antarctica; AUS, Australia; BB, Bunbury; EB, Elan Bank; IND, India; MAD, Madagascar; KPL, Kerguelen Plateau; RT, P, Perth; Rajmahal Traps; SPL, Shillong Plateau. M10 is sea-floor magnetic anomaly M10 (131.9 Ma).

6. Conclusions

Sedimentological, stratigraphic, petrological, and provenance data from the Lower Cretaceous Wölong Volcaniclastics in southern Tibet provide evidence for a volcanic event which occurred inland on the northeastern margin of Greater India. The detrital zircon U–Pb ages indicate that this volcanism probably continued from ~140 Ma to ~120 Ma. Early volcanic activity was dominated by the eruption of alkali basalts while bimodal basalt–rhyolitic/dacitic volcanics dominated the late eruptive phases. The presence of volcanic tuff particles, the fresh appearance of volcanic grains and feldspars and the angular to subangular shapes of most of volcanic and quartz grains, are indicative of rapid erosion and relatively short transport.

The alkaline character of basaltic volcanic grains and their trace and REE elements, chemical composition of detrital Cr-spinels from the Wölong Volcaniclastics all suggest a "within-plate" tectonic setting for the Early Cretaceous volcanism. Hf-isotope data show that the parent magmas of Early Cretaceous zircons were produced by the mixing of magma ascending from the mantle with partial melts derived from an older continental crust.

The Early Cretaceous magmatic event was not related to a mantle plume or large-scale continental rifting, but to the opening of deep, crust cross-cutting fractures along the northern margin of Greater India, as the regional stress-field changed as a consequence of minor anticlockwise extension when the Greater India plate began to separate from the Australia–Antarctic supercontinent. The opening of extensional fractures resulted in mantle upwelling and decompression melting, with incorporation of partial melts from an old continental crust during later stages of the volcanic activity. The volcanic activity ceased when Greater India finally separated from the Australia–Antarctica plate.

Acknowledgements

The authors thank Norman Pearson, Suzy Elhlou, Wu Bin, and Xu Xisheng for their assistance in the lab. This work benefited trough the years from numerous fruitful discussions with Profs. Wang Chengshan, Li Xianghui, Wan Xiaoqiao, Huang Zicheng, and Dr. Chen Lihui. Constructive comments from Profs. Mo Xuanxue, Zhou Meifu, J. Aitchison and Frank Thomas on early draft of the manuscript are greatly appreciated. Stimulating reviews by E. Garzanti and P. Cawood are gratefully acknowledged. This study was supported by Chinese government grants from the MOST 973 Project (2006CB701402), and NSFC Project (40302017 and 40772070), and the MOE NCET Program. Analytical data were obtained at GEMOC using instrumentation funded by ARC LIEF, and DEST Systemic Infrastructure Grants and Macquarie University. This is publication 626 from the ARC National Key Centre for Geochemical Evolution and Metallogeny of Continents (www.gemoc.mq.edu.au).

Appendix A. Method description

A1. Volcanic grains by EMPA

Fine-grained conglomerates (sample GC10) from the lower part of the Wölong Volcaniclastics were selected for polished sections with a thickness of about 200 μm. The analyses were performed at the State Key Laboratory of Mineral Deposit Research, Nanjing University, using a JXA-8800 M EMPA instrument. An accelerating voltage of 15 kV, a sample current of -1×10^{-8} A, and a defocused beam size of 40 μm were used during the experiment. 16 points were analyzed within each volcanic grain in order to get a mean major-element composition.

A2. Major and trace elements by LA-ICPMS

The laser-ablation microprobe ICPMS system at GEMOC consists of two parts: the laser-ablation microprobe sampler and the ICPMS. The laser was a custom-built microprobe based on a Quantel Brilliant Nd:YAG 266 nm laser. Ablations are carried out in He, which is mixed with Ar before entering the ICPMS torch. Analyses are carried out on an Agilent 7500s ICPMS, tuned to optimize sensitivity across the mass range from Na to U. Data reduction were done using the in-house GLITTER software (www.gemoc.mq.edu.au). Eleven major elements, 14 REEs and 18 other trace elements (V, Y, Hf, Zr, Sc, Cr, Co, Ni, Ga, Rb, Sr, Nb, Cs, Ba, Ta, Pb, Th, and U) were selected for measurement. A typical run included two analyses of the external glass standard NIST SRM 610, one analysis of the external standard basalt glass BCR-2G, ten unknown rocks, and two further analyses of the glass standard NIST SRM 610 to correct for any instrumental drift.

The laser-ablation microprobe ICPMS technique requires an external standard for calibration: such a standard is a substance that has known concentrations of the elements of interest. An internal standard, which is usually a major element, is also required to correct for differences in ablation yield and instrumental drift. For volcanic grains, we adopted Al_2O_3 as the internal standard, using values independently obtained by EMPA as described in Appendix A1. However, since most of the volcanic rocks are more or less heterogeneous in mineralogical and chemical compositions, a single internal standard for each volcanic grain is only an approximation. Thus the absolute contents of measured elements may differ from true values by 10–20%. However, the relative abundances of those elements are not affected by this level of inaccuracy in the internal standard, and can be used to interpret the nature of the volcanic rocks, especially for the discrimination of tectonic setting based on element ratios.

To test the validity of the method, we analyzed a standard basalt glass and three known basaltic and andesitic rocks using this method and compared the results with the data measured by XRF for major elements and ICPMS for trace elements (see File DR1). Our data show that this method is quite reliable and has a great potential as a tool for the study of volcaniclastic sandstone provenance.

A3. Detrital Cr-spinel by EMPA

Samples were crushed to fine grain-size (<280 μm) and then a combination of elutriation and magnetic separation techniques was used to extract a heavy mineral concentrate. Detrital Cr-spinels and zircons were hand-picked under a Nikon binocular microscope, then mounted in epoxy resin and polished to produce a smooth flat surface which exposed the interiors of the grains.

Cr-spinel compositions were determined using a JEOL JXA-8800M electron microprobe at the State Key Laboratory for Mineral Deposit Research, Nanjing University. Analysis was done under the following conditions: an accelerating voltage of 15 kV, a beam current of 20 nA, and a beam diameter of 1 μm, ZAF correction model. Counting time was 10 s for Al, Fe and Mg, 20 s for Ti, Mn, Cr, V, and Ni and 30 s for Zn. Detection limits were about 200 ppm for all elements. All Fe was reported as FeO. The ferric iron content of each analysis was determined by assuming stoichiometry, and an ideal XY_2O_4 formula, where $X=Fe^{2+}$, Mg, Ni, Mn, and Zn, and $Y=$ Cr, Al, Ti, and Fe^{3+}, following the methods described by Barnes and Roeder (2001).

A4. Detrital zircon U–Pb dating by LA-ICPMS

The samples were crushed to a fine grain-size and conventional magnetic and heavy liquid separation techniques were used to extract a zircon-rich heavy mineral concentrate. Zircons of different size, color and morphology were hand-picked under a Leica binocular microscope, mounted in epoxy disks and polished to expose their cores. BSE/CL imaging, U–Pb dating and Hf-isotope analysis for samples GC09 and GC10 are carried out at the GEMOC Key Centre of Macquarie University, Australia, while U–Pb dating for samples GCQ, GC-H7, and GCL11 are analyzed at the State Key Laboratory for

Mineral Deposit Research, Nanjing University. BSE/CL imaging was done using a CAMECA-SX100 electron microprobe at an accelerating voltage of 15 kV and a beam current of 15–20 nA. These images were used to select spots for U–Pb and Hf-isotope analyses. Zircon U–Pb dating was performed using an Agilent HP 4500 ICPMS, attached to a Merchantek/NWR 213 mm laser-ablation microprobe. Each run comprises ca. 10 unknown sample analyses and four GJ-1 zircon standards (added at the beginning and the end of the run). Two well-characterized zircons (91500 and Mud Tank) were also analyzed to control reproducibility and instrument stability. Laser-ablation spot diameter was ~30 μm. Analytical results were calculated using the GLITTER 4.4 program (Griffin et al., 2008). Comparison of count rates between sample and standard also yields concentration values for U and Th. Detailed analytical procedures, precision and accuracy are described by Jackson et al. (2004). U–Pb isotopic results were corrected for common Pb using the program Com-PbCorr#3_16f1 of Andersen (2002). None of the grains reported here required significant correction. The corrected isotopic ratios were calculated using ISOPLOT program v.2.49 (Ludwig, 2001). Results described in this paper exclude analyses with ≥20% discordance, but greater discordance was accepted for the Early Cretaceous zircon grains because of the imprecision of the $^{207}Pb/^{206}Pb$ ages in these young grains. $^{207}Pb/^{206}Pb$ ages were used for grains with ages >1000 Ma, and $^{206}Pb/^{238}U$ ages for younger zircons.

A5. Detrital zircon Lu–Hf isotope analyses by MC-ICPMS

Lu–Hf isotope analyses were performed using a Nu Plasma MC-ICPMS with a Merchantek/NWR 213 mm laser-ablation microprobe. Typical ablation time is 30 to 120 s, resulting in pits 20–60 μm deep. Before analyses of unknown samples, zircons 91500 and Mud Tank were analyzed to check instrument reliability and stability. The analytical conditions and procedures were similar to those described by Griffin et al. (2000).

To calculate model ages (T_{DM}) and epsilon Hf, we have adopted a depleted mantle model with $^{176}Hf/^{177}Hf = 0.28325$ and $^{176}Lu/^{177}Hf = 0.0384$ and chondrite values for $^{176}Hf/^{177}Hf = 0.282772$ and $^{176}Lu/^{177}Hf = 0.0332$ (Griffin et al., 2000). The decay constant of ^{176}Lu applied in this paper is 1.867×10^{-11} per year (Söderlund et al., 2004).

T_{DM} ages, which are calculated using the measured $^{176}Lu/^{177}Hf$ of the zircon, can only give a minimum age for the source rocks of the magma from which the zircon crystallized. Therefore we also have calculated, for each zircon, a "crustal" model age on, (T^{C}_{DM}) which assumes that its parental magma was produced from an average continental crust ($^{176}Lu/^{177}Hf = 0.015$; GERM database) that originally was derived from the depleted Hf mantle (Griffin et al., 2000).

$$\varepsilon Hf(0) = 10000 * [(^{176}Hf/^{177}Hf)_S / (^{176}Hf/^{177}Hf)_{CHUR,0} - 1]$$

$$\varepsilon Hf(t) = 10000 * \{[(^{176}Hf/^{177}Hf)_S - (^{176}Lu/^{177}Hf)_S * (e^{\lambda t} - 1)] \div [(^{176}Hf/^{177}Hf)_{CHUR,0} - (^{176}Lu/^{177}Hf)_{CHUR} * (e^{\lambda t} - 1)] - 1\}$$

$$T_{DM1} = 1/\lambda * \ln\{1 + [(^{176}Hf/^{177}Hf)_S - (^{176}Hf/^{177}Hf)_{DM}] \div [(^{176}Lu/^{177}Hf)_S - (^{176}Lu/^{177}Hf)_{DM}]\}$$

$$T_{DM2} = T_{DM1} - (T_{DM1} - t) * [(f_{cc} - f_s) / (f_{cc} - f_{DM})] f_{Lu/Hf} = (^{176}Lu/^{177}Hf)_S / (^{176}Lu/^{177}Hf)_{CHUR} - 1$$

where, $\lambda = 1.867 \times 10^{-11}$ year^{-1} (Söderlund et al., 2004); $(^{176}Lu/^{177}Hf)_S$ and $(^{176}Hf/^{177}Hf)_S$ are the measured values of the samples; $(^{176}Lu/^{177}Hf)_{CHUR} = 0.0332$ and $(^{176}Hf/^{177}Hf)_{CHUR,0} = 0.282772$ (BlichertToft and Albarede, 1997); $(^{176}Lu/^{177}Hf)_{DM} = 0.0384$ and $(^{176}Hf/^{177}Hf)_{DM} = 0.28325$ (Griffin et al., 2000); $(^{176}Lu/^{177}Hf)_{mean\ crust} = 0.015$; $f_{cc} = [(^{176}Lu/^{177}Hf)_{mean\ crust}/(^{176}Lu/^{177}Hf)_{CHUR}] - 1$; $f_s = f_{Lu/Hf}$; $f_{DM} = [(^{176}Lu/^{177}Hf)_{DM}/(^{176}Lu/^{177}Hf)_{CHUR}] - 1$; t = crystallization time of zircon.

Appendix B. Supplementary data

Supplementary data associated with this article can be found, in the online version, at doi:10.1016/j.sedgeo.2009.11.008.

References

Ali, J.R., Aitchison, J.C., 2005. Greater India. Earth Science Reviews 72 (3–4), 169–188.
Ali, J.R., Aitchison, J.C., 2008. Gondwana to Asia: plate tectonics, paleogeography and the biological connectivity of the Indian sub-continent from the Middle Jurassic through latest Eocene (166–35 Ma). Earth Science Reviews 88 (3–4), 145–166.
Andersen, T., 2002. Correction of common lead in U–Pb analyses that do not report ^{204}Pb. Chemical Geology 192 (1–2), 59–79.
Arai, S., 1992. Chemistry of chromian spinel in volcanic rocks as a potential guide to magma chemistry. Mineralogical Magazine 56, 173–184.
Barnes, S.J., Roeder, P.J., 2001. The range of spinel compositions in terrestrial mafic and ultramafic rocks. Journal of Petrology 42 (12), 2279–3202.
Bertle, R.J., Suttner, T.J., 2005. New biostratigraphic data for the Chikkim Formation (Cretaceous, Tethyan Himalaya, India). Cretaceous Research 26 (6), 882–894.
BlichertToft, J., Albarede, F., 1997. The Lu–Hf isotope geochemistry of chondrites and the evolution of the mantle–crust system. Earth and Planetary Science Letters 148 (1–2), 243–258.
Bordet, P., Colchen, M., Le Fort, P., Mouterde, R., Remy, M., 1967. Données nouvelles sur la géologie de la Thakkhola (Himalaya du Nepal). Bull. Soc. Géol France 7 (9), 883–896.
Cawood, P.A., Johnson, M.R.W., Nemchin, A.A., 2007. Early Palaeozoic orogenesis along the Indian margin of Gondwana: tectonic response to Gondwana assembly. Earth and Planetary Science Letters 255 (1–2), 70–84.
Chen, L., Hu, X., Huang, Z., 2007. Constrains from Early Cretaceous volcaniclastic sandstones in southern Tibet on a volcanic event in the northern margin of the Indian Continent. Dizhi Xuebao 81 (4), 501–510 (in Chinese with English abstract).
Coffin, M.F., et al., 2002. Kerguelen hotspot magma output since 130 Ma. Journal of Petrology 43 (7), 1121–1139.
Dabard, M.-P., Chauvel, J.-J., Loi, A., 1994. Compositional affinities of volcanic fragments in sedimentary rocks using electron microprobe analysis. Sedimentary Geology 88 (3–4), 283–299.
Davies, H.L., et al., 1989. Basalt basement from the Kerguelen Plateau and the trail of a Dupal plume. Contributions to Mineralogy and Petrology 103 (457–469).
Dick, H.J.B., Bullen, T., 1984. Chromian spinel as a petrogenetic indicator in abyssal and alpine-type peridotites and spatially associated lavas. Contribution to Mineralogy and Petrology 86 (54–76).
Dickinson, W.R., 1985. Interpreting provenance relations from detrital modes of sandstones. NATO ASI Series. Series C. Mathematical and Physical Sciences 148, 333–361.
Dürr, S.B., Gibling, M.R., 1994. Early Cretaceous volcaniclastic and quartzose sandstones from north central Nepal: composition, sedimentology and geotectonic significance. Geologische Rundschau 83 (1), 62–75.
Floyd, P.A., Winchester, J.A., 1978. Identification and discrimination of altered and metamorphosed volcanic rocks using immobile elements. Chemical Geology 21, 291–306.
Gaetani, M., et al., 1986. Stratigraphy of the Tethys Himalaya in Zanskar, Ladakh. Rivista Italiana di Paleontologia e Stratigrafia 91, 443–478.
Gaina, C., Müller, R.D., Brown, B., Ishihara, T., 2003. Microcontinent formation around Australia. In: Hillis, R.R., Müller, R.D. (Eds.), Evolution and Dynamics of the Australian Plate. Geological Society of America, Boulder, USA, pp. 40–416.
Gaina, C., Müller, R.D., Brown, B., Ishihara, T., Ivanov, S., 2007. Breakup and early seafloor spreading between India and Antarctica. Geophysical Journal International 170 (1), 151–169.
Gansser, A., 1964. Geology of the Himalayas. Interscience Publishers John Wiley and Sons, New York.
Garzanti, E., 1991. Stratigraphy of the Early Cretaceous Giumal Group (Zanskar Range, northern India). Rivista Italiana di Paleontologia e Stratigrafia 97 (3–4), 485–509.
Garzanti, E., 1993. Sedimentary evolution and drowning of a passive margin shelf (Giumal Group; Zanskar Tethys Himalaya, India): palaeoenvironmental changes during final break-up of Gondwanaland. Geological Society Special Publications 74, 277–298.
Garzanti, E., 1999. Stratigraphy and sedimentary history of the Nepal Tethys Himalaya passive margin. Journal of Asian Earth Sciences 17 (5–6), 805–827.
Garzanti, E., Casnedi, R., Jadoul, F., 1986. Sedimentary evidence of a Cambro–Ordovician orogenic event in the northwestern Himalaya. Sedimentary Geology 48 (3–4), 237–265.
Garzanti, E., Vezzoli, G., Andò, S., Castiglioni, G., 2001. Petrology of rifted-margin sand (Red Sea and Gulf of Aden, Yemen). Journal of Geology 109 (3), 277–297.
Gehrels, G.E., et al., 2003. Initiation of the Himalayan Orogen as an early Paleozoic thin-skinned thrust belt. GSA Today 13 (9), 4–9.
Gehrels, G.E., DeCelles, P.G., Ojha, T.P., Upreti, B.N., 2006. Geologic and U–Th–Pb geochronologic evidence for early Paleozoic tectonism in the Kathmandu thrust sheet, central Nepal Himalaya. Geological Society of America Bulletin 118 (1–2), 185–198.
Gibling, M.R., et al., 1994. Early Cretaceous strata of the Nepal Himalayas: conjugate margins and rift volcanism during Gondwanan breakup. Journal of the Geological Society of London 151 (Part 2), 269–290.
Gradstein, F.M., et al., 1991. Mesozoic Tethyan strata of Thakkhola, Nepal: evidence for the drift and breakup of Gondwana. Palaeogeography, Palaeoclimatology, Palaeoecology 88 (3–4), 193–218.

Gradstein, F.M., Ogg, J.G., Smith, A.G., Agterberg, F.P., Bleeker, W., et al., 2004. A Geologic Time Scale 2004. Cambridge University Press, p. 589.
Griffin, W.L., et al., 2000. The Hf isotope composition of cratonic mantle: LAM-MC-ICPMS analysis of zircon megacrysts in kimberlites. Geochimica et Cosmochimica Acta 64 (1), 133–147.
Griffin, W.L., Powell, W.J., Pearson, N.J., O'Reilly, S.Y., 2008. GLITTER: data reduction software for laser ablation ICP-MS. In: Sylvester, P. (Ed.), Laser Ablation-ICP-MS in the Earth Sciences: Mineralogical Association of Canada Short Course Series, vol. 40, pp. 204–207. Appendix 2.
Heine, C., Mueller, R.D., Gaina, C., 2004. Reconstructing the lost eastern Tethys ocean basin: convergence history of the SE Asian margin and marine gateways. Geophysical Monograph 149, 37–54.
Hodges, K.V., 2000. Tectonics of the Himalaya and southern Tibet from two perspectives. Geological Society of America Bulletin 112 (3), 324–350.
Hu, X.M., Wang, C.S., Li, X.H., Luba, J., 2006. Upper Cretaceous oceanic red beds in southern Tibet: Lithofacies, environments and colour origin. Science in China Series D-Earth Sciences 49 (8), 785–795 (in Chinese with English abstract).
Hu, X., Jansa, L., Wang, C., 2008. Upper Jurassic–Lower Cretaceous stratigraphy in south-eastern Tibet: a comparison with the western Himalayas. Cretaceous Research 29 (2), 301–315.
Jackson, S.E., Pearson, N.J., Griffin, W.L., Belousova, E.A., 2004. The application of laser ablation-inductively coupled plasma-mass spectrometry to *in situ* U/Pb zircon geochronology. Chemical Geology 211 (1–2), 47–69.
Jadoul, F., Berra, F., Garzanti, E., 1998. The Tethys Himalayan passive margin from late Triassic to early Cretaceous (South Tibet). Journal of Asian Earth Sciences 16 (2–3), 173–194.
Kamenetsky, V.S., Crawford, A.J., Meffre, S., 2001. Factors controlling chemistry of magmatic spinel: an empirical study of associated olivine, Cr-spinel and melt inclusions from primitive rocks. Journal of Petrology 42, 655–671.
Kent, R.W., Saunders, A.D., Kempton, P.D., Ghose, N.C., 1997. Rajmahal basalts, Eastern India: mantle sources and melt distribution at a volcanic rifted margin. In: Mahoney, J.J., Coffin, M.F. (Eds.), Large igneous provinces: continental, oceanic and planetary flood volcanism: Geophysical Monograph, American Geophysical Union, vol. 100, pp. 145–182.
Kent, R.W., Pringle, M.S., Mueller, R.D., Saunders, A.D., Ghose, N.C., 2002. $^{40}Ar/^{39}Ar$ geochronology of the Rajmahal basalts, India, and their relationship to the Kerguelen Plateau. Journal of Petrology 43 (7), 1141–1153.
Kumar, S., Singh, I.B., Singh, S.K., 1977. Lithostratigraphy, structure, depositional environment, palaeocurrent and trace fossils of the Tethyan sediments of Molla Johar area, Pithoragarh–Chamoli Districts, Uttar Pradesh, India. Journal of Palaeontologica Society of India 20, 396–435.
Le Maitre, R.W., et al., 1989. A Classification of Igneous Rocks and Glossary of Terms. Blackwell, Oxford, p. 193.
Leckie, R.M., Bralower, T.J. and Cashman, R., 2002. Oceanic anoxic events and plankton evolution; biotic response to tectonic forcing during the Mid-Cretaceous. Paleoceanography, 17(3). doi:10.1029/2001PA000623.
Leech, M.L., Singh, S., Jain, A.K., Klemperer, S.L., Manickavasagam, R.M., 2005. The onset of India–Asia continental collision: early, steep subduction required by the timing of UHP metamorphism in the western Himalaya. Earth and Planetary Science Letters 234 (1–2), 83–97.
Lenaz, D., Kamenetsky, V.S., Crawford, A.J., Princivalle, F., 2000. Melt inclusions in detrital spinel from the SE Alps (Italy–Slovenia): a new approach to provenance studies of sedimentary basins. Contributions to Mineralogy and Petrology 139 (6), 748–758.
Liu, G., Einsele, G., 1994. Sedimentary history of the Tethyan basin in the Tibetan Himalayas. Geologische Rundschau 83 (1), 32–61.
Ludwig, K.R., 2001. User's Manual for Isoplot/Ex rev. 2.49, A Geochronological Toolkit for Microsoft Excel. Berkeley Geochronology Center Special Publication 1, 1–55.
Manspeizer, W., 1988. Triassic–Jurassic rifting and opening of the Atlantic: An Overview. In: Manspeizer, W. (Ed.), Triassic–Jurassic Rifting, Continental Breakup and the Origin of the Atlantic Ocean and Passive margins. Elsevier, pp. 41–80.
Meschede, M., 1986. A method of discriminating between different types of mid-ocean ridge basalts and continental tholeiites with the Nb–Zr–Y diagram. Chemical Geology 56, 207–218.
Mihut, D., Müller, R.D., 1998. Volcanic margin formation and Mesozoic rift propagators in the Cuvier Abyssal Plain off Western Australia. Journal of Geophysical Research 103, 27,135–27,150.
Müller, R.D., Mihut, D. and Baldwin, S., 1998. A new kinematic model for the formation and evolution of the West and Northwest Australian Margin. In: P.G. Purcell and R.R. Purcell (Editors), The sedimentary basin of Western Australia 2, Proceedings of the Petroleum Exploration Society of Australia Symposium, Perth, Western Australia, pp. 55-71.
Myrow, P.M., et al., 2009. Stratigraphic correlation of Cambrian–Ordovician deposits along the Himalaya: implications for the age and nature of rocks in the Mount Everest region. Geological Society of America Bulletin 121, 323–332.
Nagy, J., Gradstein, F.M., Gibling, M.R., Thomas, F.C., 1995. Foraminiferal stratigraphy and paleoenvironments of Late Jurassic to Early Cretaceous deposits in Thakkhola, Nepal. Micropaleontology 41 (2), 143–170.
Najman, Y., et al., 2008. The Paleogene record of Himalayan erosion: Bengal Basin, Bangladesh. Earth and Planetary Science Letters 273 (1–2), 1–14.
Pearce, J.A., Cann, J.R., 1973. Tectonic setting of basic volcanic rocks determined using trace element analysis. Earth and Planetary Science Letters 19, 290–300.
Powell, C.M., Roots, S.R., Veevers, J.J., 1988. Pre-breakup continental extension in East Gondwanaland and the early opening of the eastern Indian Ocean. Tectonophysics 155 (1–4), 261–283.
Premoli Silva, I., Garzanti, E., Gaetani, M., 1991. Stratigraphy of the Chikkim and Fatu La formations in the Zangla and Zumlung units (Zanskar Range, India) with comparisons to the Thakkhola region (central Nepal): Mid-Cretaceous evolution of the Indian passive margin. Rivista Italiana di Paleontologia e Stratigrafia 97 (3–4), 511–564.
Ramana, M.V., Ramprasad, T., Desa, M., 2001. Seafloor spreading magnetic anomalies in the Enderby Basin, East Antarctica. Earth and Planetary Science Letters 191 (3–4), 241–255.
Ratschbacher, L., Frisch, W., Liu, G., Chen, C., 1994. Distributed deformation in southern and western Tibet during and after the India–Asia collision. Journal of Geophysical Research 99, 19,917–19,945.
Sakai, H., 1983. Geology of the Tansen group of the lesser Himalaya in Nepal. Memoirs of the Faculty of Science, Kyushu University, Series D, Geology, 25, 27–74.
Sakai, H., Hamamoto, R., Arita, K., 1992. Radiometric ages of alkaline volcanic rocks from the upper Gondwana of the lesser Himalayas, west central Nepal, and their tectonic significance. : Bulletin of the Department of Geology, vol. 2. Tribhuvan University, Kathmandu, pp. 65–74.
Sciunnach, D., Garzanti, E., 1997. Detrital chromian spinels record tectono-magmatic evolution from Carboniferous rifting to Permian spreading in Neotethys. Ofioliti 22, 101–110.
Sinha, A., 1989. Geology of the Higher Central Himalaya. John Wiley and Sons, New York. 219 pp.
Söderlund, U., Patchett, P.J., Vervoort, J.D., Isachsen, C.E., 2004. The ^{176}Lu decay constant determined by Lu–Hf and U–Pb isotope systematics of Precambrian mafic intrusions. Earth and Planetary Science Letters 219 (3–4), 311–324.
Sun, S.S., McDonough, W.F., 1989. Chemical and isotope systematics of oceanic basalts: implications for mantle composition and processes. In: Saunders, A.D. (Ed.), Magmatism in Ocean Basins. Geological Society Publication, pp. 313–345.
Symonds, P.A., Planke, S., Frey, O. and Skogseid, J., 1998. Volcanic evolution of the western Australian continental margin and its implications for basin development. In: P.G. Purcell and R.R. Purcell (Editors), The sedimentary basin of Western Australia 2. Proceedings of the Petroleum Exploration Society of Australia Symposium, Perth, Western Australia, pp. 33–54.
Willems, H., Zhou, Z., Zhang, B., Grafe, K.U., 1996. Stratigraphy of the Upper Cretaceous and Lower Tertiary Strata in the Tethyan Himalayas of Tibet (Tingri area, China). Geologische Rundschau 85 (4), 723–754.
Wu, Y.B., Zheng, Y.F., 2004. Genesis of zircon and its constraints on interpretation of U–Pb age. Chinese Science Bulletin 49, 1554–1569.
Yin, J., Enay, R., 2004. Tithonian ammonoid biostratigraphy in eastern Himalayan Tibet. Geobios 37 (5), 667–686.
Zhu, T., Zou, G. and Zhou, M., 2002. 1:250,000 geological map of the Nyalam area, Tibet Chengdu Institute of Geology and Mineral Resources, China Geological Survey. (in Chinese)
Zhu, B., Kidd, W.S.F., Rowley, D.B., Currie, B.S., 2004. Chemical compositions and tectonic significance of chrome-rich spinels in the Tianba Flysch, southern Tibet. Journal of Geology 112 (4), 417–434.
Zhu, B., Delano, J.W., Kidd, W.S.F., 2005a. Magmatic compositions and source terranes estimated from melt inclusions in detrital Cr-rich spinels: an example from mid-Cretaceous sandstones in the eastern Tethys Himalaya. Earth and Planetary Science Letters 233 (3–4), 295–309.
Zhu, D.C., Pan, G.T., Mo, X.X., Wang, L.Q., Liao, Z.L., Jiang, X.S., Geng, Q.R., 2005b. SHRIMP U–Pb zircon dating for the dacite of the Sangxiu Formation in the central segment of Tethyan Himalaya and its implications. Chinese Science Bulletin 50 (6), 563–568.
Zhu, D.C., Mo, X.X., Liao, Z.L., Jiang, X.S., Wang, L.Q., Zhao, Z.D., 2007. Petrogenesis of volcanic rocks in the Sangxiu Formation, central segment of Tethyan Himalaya: a probable example of plume–lithosphere interaction. Journal of Asian Earth Sciences 29 (2–3), 320–335.
Zhu, D.C., Mo, X.X., Pan, G.T., Zhao, Z.D., Dong, G.C., Shi, Y.R., Liao, Z.L., Wang, L.Q., Zhou, C.Y., 2008. Petrogenesis of the earliest Early Cretaceous mafic rocks from the Cona area of the eastern Tethyan Himalaya in south Tibet: interaction between the incubating Kerguelen plume and the eastern Greater India lithosphere? Lithos 100 (1–4), 147–173.